A comprehensive kinetic study of the combustion mechanism of methyl isocyanate

Jonathan Honorien, Baptiste Sirjean, Pierre-Alexandre Glaude, René Fournet

A comprehensive kinetic study of the combustion mechanism of methyl isocyanate

Jonathan Honorien[1], Baptiste Sirjean[1], Pierre-Alexandre Glaude[1], René Fournet[1,*]

[1] Université de Lorraine, CNRS, LRGP, F-54000 Nancy, France

Corresponding author :

René Fournet

Laboratoire Réactions et Génie des Procédés

1 rue Grandville BP 20451 54001 Nancy Cedex,

France

Email: rene.fournet@univ-lorraine.fr

A comprehensive kinetic study of the combustion mechanism of methyl isocyanate

Jonathan Honorien[1], Baptiste Sirjean[1], Pierre-Alexandre Glaude[1], René Fournet[1,*1]

[1] Université de Lorraine, CNRS, LRGP, F-54000 Nancy, France

Abstract: A detailed mechanism for the combustion of methyl isocyanate is proposed for the first time. Electronic structures were calculated at the CCSD(T)/cc-VTQ∞Z//B2PLYP-D3/6-311++G(3df,2pd) level of theory to investigate potential energy profiles and used in reaction rate theories to compute rate coefficients. The mechanism contains 130 reactions and was merged with the reaction base proposed by Glarborg et al.[1] for light hydrocarbons and nitrogen-containing species. Experimental data related to the pyrolysis of methyl isocyanate were simulated in a closed reactor and a good agreement was observed for all the species profiles reported. Similarly, the auto-ignition temperature (Ti_{gn}) of methyl isocyanate was calculated based on the standard ASTME659-78 test, and led to a value close to the experimental value. Flow rate and sensitivity analysis were performed under pyrolysis and combustion conditions in order to highlight the main reaction pathways.

Keywords: Methyl isocyanate; Kinetics; Detailed Mechanism; Pyrolysis; Combustion.

1. Introduction

Isocyanates are a class of highly reactive molecules used in chemical and pharmaceutical industries, as well as in the production of pesticides. For instance, isocyanates are involved in the manufacturing of polyurethanes [2] which are mainly used as foams, fibers, rubbers, adhesives or coatings in automobile industry, furnishings and building insulation materials. Due to their high toxicity[2], isocyanates should be handled with care. In 1984, methyl isocyanate was responsible for the worst industrial disaster ever happened and caused the death of more than 20,000 people in Bhopal [3, 4]. Isocyanates such as methyl isocyanate or isocyanic acid can also be found in atmosphere, as emission of biomass burning[5] or, more generally, as intermediates in the thermal degradation of nitrogen containing organic compounds (incineration, pyrolysis, accidental fire, *etc.*) [2, 6-8]. Recent interest in the valorization of solid recovered fuels, such as manufactured wood or plastics can also be

[1] Corresponding author E-Mail: rene.fournet@univ-lorraine.fr

a source of isocyanate emissions when thermal processes are used [9-14]. The low or moderate temperature reactivity of isocyanates has been widely investigated from the 1960s, in order to develop materials for industrial applications [15, 16]. In contrast, their high temperature reactivity remains poorly studied and, from our knowledge, no detailed kinetics mechanism has been proposed in the literature to model the thermal degradation of isocyanates at high temperature. In 1982, Blake and Ijadi-Maghsoodi[17] published an experimental study of the pyrolysis of methyl isocyanate (MIC) in a batch reactor, for temperatures ranging from 700 to 821 K. They observed HCN, H_2 and CO as major products and they showed that N,N'-dimethylcarbodiimide is an intermediate for the initiation of MIC pyrolysis. They proposed a simplified mechanism based on radical chain reactions to explain the formation of observed products and they derived global rate constants and reaction orders from experiments. In 1983, Blake and Ijadi-Maghsoodi[18] extended their work to the pyrolysis of larger alkyl-isocyanates: ethyl, isopropyl and ter-butyl isocyanates. They experimentally observed that the reactions involved in the reactant consumption differ according to the size of the alkyl chains. Indeed, the authors showed that concerted reactions involving a six-centered transition state compete with radical reactions and become prominent when the size of the alkyl group increases. In 1996, Sonya et al.[19] experimentally studied the pyrolysis of para-toluene isocyanate, an intermediate in the thermal degradation of di-isocyanates. The experiments were carried out in a flow reactor at temperatures ranging from 823 to 873K. They detected major products such as benzonitrile compounds, phenylisocyanate, toluene and benzene and they derived rate constants and reaction orders. They also proposed possible reaction pathways to explain their formation.

In this paper, we explored the reaction pathways involved in the thermal degradation of methyl isocyanate and we propose a detailed kinetic mechanism, based on electronic structure calculations performed at the CCSD(T)/cc-VTQ∞Z//B2PLYP-D3/6-311++G(3df,2pd) level of theory. Pressure effects have been taken into account for specific unimolecular reactions and reaction rate parameters have been deduced from reaction rate theories. The proposed mechanism was confronted with the available experimental data, *i.e.*, species profiles in pyrolysis and the prediction of auto-ignition temperature (AIT) which is a global combustion data.

2. Computational Methods

For all the molecular structures considered in this study, we calculated the geometry optimization and harmonic vibrational frequencies by means of the B2PLYP[20] double-hybrid density functional, coupled with D3 empirical correction [21] and the extended 6-311++G(3df,2pd) basis set. It has been shown that this functional provides more accurate harmonic frequencies than classical DFT approaches, such as B3LYP[22]. Energy calculations were performed at the CCSD(T) level of theory

combined with a complete basis set extrapolation (CBS) using the augmented aug-cc-pVTZ and aug-cc-pVQZ Dunning basis sets. For reactions involving a number of heavy atoms larger than 6, diffuse functions were not considered in order to reduce the computational cost. All the calculations were performed with the Gaussian 16 program package[23].

Internal rotations around simple bonds were treated as hindered rotor using the 1D-HR formalism[24] rather than harmonic oscillators. To avoid possible coupling effects between vibration modes computed from Gaussian16, we modified the classical 1D-HR treatment. In fact, the harmonic frequency corresponding to an internal rotation is computed from the relaxed scan (rather than removed from the Gaussian list) and its partition function is replaced by that calculated from the 1D-HR calculation[25]. Relaxed scans were systematically performed at the B2PLYP-D3/6-311+G(2d,p). Tunneling effect, based on a one-dimensional asymmetric Eckart potential, was taken into account for reactions involving a H-atom transfer. Usually, this approach leads to accurate transmission coefficients for temperatures above 500 K[26, 27]. Statistical factor involving external symmetries (previously removed from rotational partition functions) and optical isomers of reactants and transition states (TS) were also considered to correctly compute the rate constants. Finally, high-pressure limit rate constants were computed from canonical transition state theory and fitted over the temperature range 500-2000 K, using a three parameters Arrhenius equation (equation 1):

$$k_{\infty}(T) = A\,T^{n}e^{-\frac{E}{RT}} \qquad \text{(eq.1)}$$

All these calculations, as well as thermodynamic data (S°_{298K} and $C_p^{\circ}(T)$) and NASA polynomials determination were automatically performed with the in-house code THERMROT[25]. Even if enthalpies of formation can be computed from THERMROT using atomization energies, we evaluated them from isodesmic reactions using experimental data found in the CCCBDB[28] data base or in the active thermochemical tables (ATcT[29]).

Pressure effects for sensitive reactions, such as H-atom additions, β-scissions or H-atom transfers were processed by means of RRKM-Master equation using the MESS code of the PAPR suite[30] and fitted with the PLOG formalism used in the Chemkin Pro software[31]. Lennard-Jones parameters were computed using the formalism developed by Tee et al. [32] which requires the knowledge of critical pressure (P_C), temperature (T_C) and the acentric factor (ω). For unknown data (T_C, P_C and ω), an estimation has been performed from the group-contribution method proposed by Marrero and Gani [33]. N_2 was chosen as bath gas and an exponential down model, defined by equation 2, was considered to take into account energy collisional energy transfer according to reference[34].

$$\Delta E_{down} = 250\left(\frac{T}{300}\right)^{0.85} cm^{-1} \qquad \text{(eq.2)}$$

For specific reactions involving the formation of van der Waals complexes, a variational treatment was applied and the rate constants were derived from phase space theory using the MESS code[30].

3. Results and discussion

3.1 Description of the Mechanism

In this section, we describe the main elementary reactions considered in the combustion mechanism of methyl isocyanate. This mechanism was constructed by considering all energetically favorable pathways involved in the combustion of methyl isocyanate. This set of reactions has been merged with the mechanism proposed by Glarborg et al.[1] to describe the combustion chemistry of light nitrogen and hydrocarbon species.

3.1.1 Primary reactions of CH_3NCO

- ***Initiation reactions***

Unimolecular initiations, involving the formation of two free radicals can often be selected based on the bond dissociation energies (BDE). To our knowledge, no BDE for methyl isocyanate is available in the literature. Figure 1 depicts the BDE for the C-N and C-H bonds, calculated at the CCSD(T)/aug-cc-VTQ∞Z//B2PLYP-D3/6-311++G(3df,2pd) level of theory. As shown in figure 1, the values obtained are high which makes the corresponding unimolecular initiations difficult. Compared to alkylamines, the BDE of the C-N bond in methyl isocyanate is higher than that involves in methylamine (85.7 kcal mol^{-1} [35]). In contrast, the removal of a hydrogen atom yields to a close value (93.9 kcal mol^{-1} for methylamine[35]).

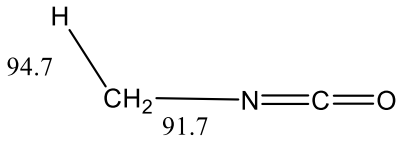

Fig 1. Bond dissociation energies of the CH_3-N and C-H bonds in MIC, in kcal mol^{-1}.

Even if the unimolecular initiations involve high bond dissociation energies, they were considered in the mechanism and the reactions have been written in the reverse direction, *i.e.*, from termination between two radicals. The rate coefficients of these barrierless reactions have been deduced from correlations proposed in the EXGAS software[36].

Initiations can also occur by bimolecular H-atom abstraction with O_2, according to the reaction R1:

$$CH_3NCO + O_2 = \bullet CH_2NCO + HO_2\bullet \quad (R1)$$

As mentioned by Zhou et al.[37], such reaction involves the formation of complexes related to the reactant (RC) and the product (PC). In order to take into account the effect of these complexes, we performed a complete calculation of the potential energy profile (Figure 2) and we compared the rate constant with that obtained without considering the formation of the complexes. All the calculations were performed considering the triplet state of O_2. The rate constants related to the formation of the complexes have been estimated by phase space theory, using the formalism proposed in the MESS code[30] for barrierless reactions. To this end, relaxed scans were performed from the center of mass of each fragments, at the B2PLYP-D3/6-311++G(3df,2pd) level of theory. Then, potential energy was fitted from a power law expansion as a function of distance R between the centers of mass:

$$V = -\frac{C}{R^n} \qquad \text{(eq.3)}$$

We also investigated the addition of O_2 on the carbon atom bearing the double bond. This reaction involves a barrier height of 55.9 kcal mol^{-1} and yields to the formation of a diradical (in triplet state). In their study on the modelling of nitrogen chemistry, Glarborg et al.[1] considered a similar reaction between O_2 and isocyanic acid (HNCO), leading to the formation of CO_2 and nitroxyl (HNO). The estimated energy barrier was equal to 58.9 kcal mol^{-1} in accordance with the value obtained in this work.

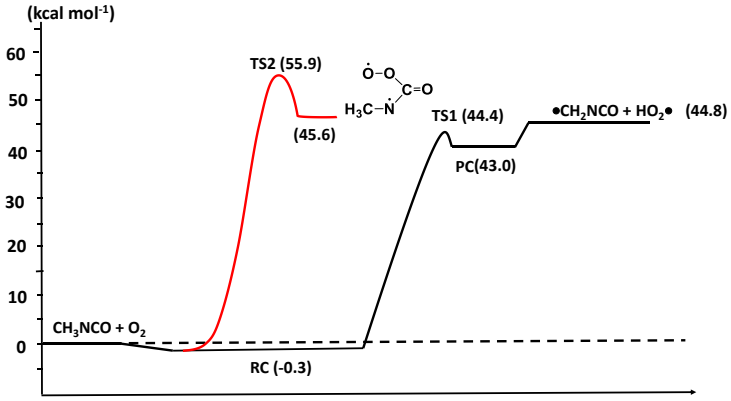

Fig 2. Potential energy profile of bimolecular initiations involving O_2 (triplet). E_{0K+ZPE} are given in kcal mol^{-1}.

If several reaction pathways are possible for the diradical, such as ring closure or H-shift, we did not further investigate these reactions because the first step does not compete with the abstraction of the hydrogen atom by O_2 (Figure 3). In addition, it can be noted in Figure 3 that the effect of pre-reactive complexes is little marked. This can be explained by the weak energy differences between the complexes and the reactants or products.

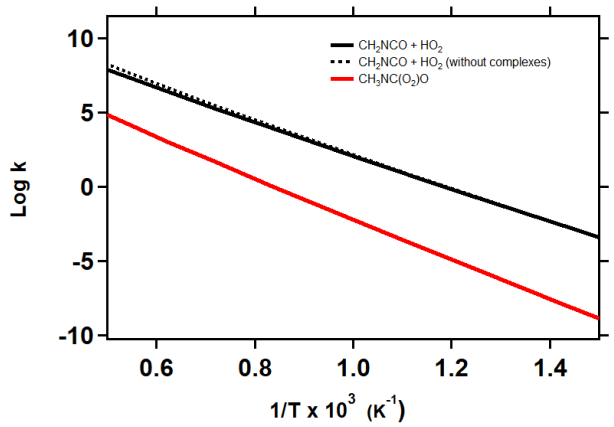

Fig 3. Plot of the rate constants for the reactions of $CH_3NCO + O_2$.

As already discussed, unimolecular radical initiations involve high activation energies. In the case of MIC, it is also possible to consider concerted molecular reactions. Figure 4 summarizes the main reaction pathways investigated in this study.

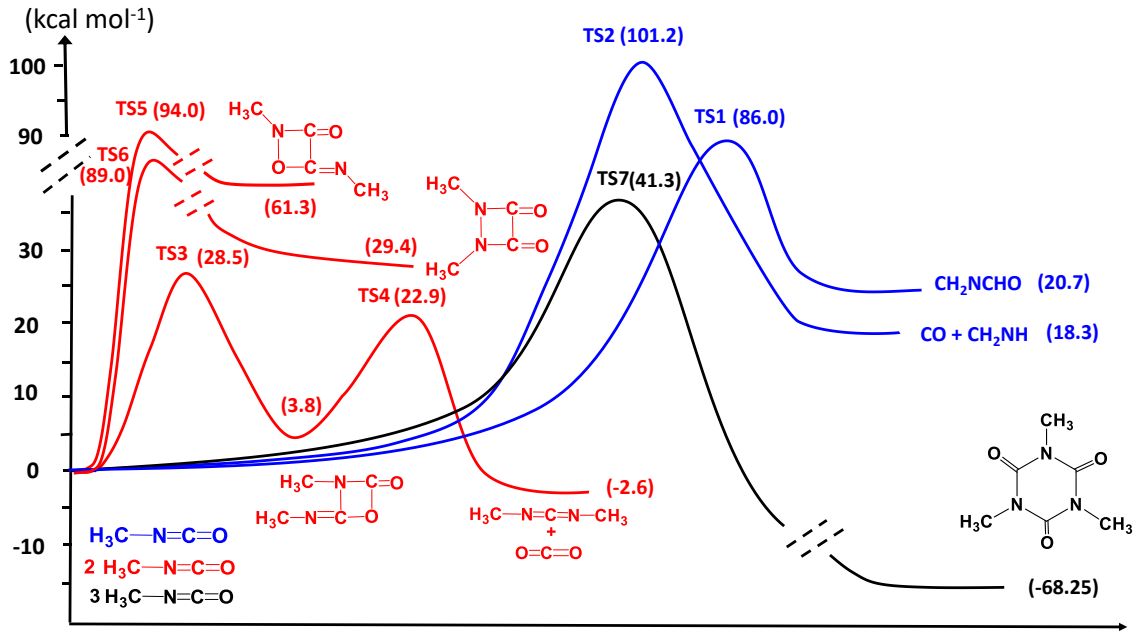

Fig 4. Potential energy profile related to concerted reactions of CH_3NCO. E_{0K+ZPE} are given in kcal mol^{-1}.

We first considered unimolecular concerted reactions (blue paths in figure 4). The first reaction implies a four-centered transition state (TS1) with a H-transfer between the two carbon atoms and a shift of the double bond between the carbon and the nitrogen atom. This reaction yields to the formation of N-methylideneformamide (CH_2NCHO). The second pathway (TS2) involves a H-shift between the carbon and the nitrogen atoms and yields to carbon monoxide and methanimine (CH_2NH). The energy barrier of the first reaction is close to those involved in free radical initiations, whereas the

second one has a much higher activation energy. Furthermore, entropic contributions disfavor concerted reactions over radical reactions, so they were not retained in the final mechanism.

The presence of an isocyanate function can lead to additions on the different double bonds. We considered cycloadditions between the carbon, oxygen and nitrogen atoms (red paths in figure 4) of two isocyanate molecules. A first possibility involves the four-centered addition between the carbon and oxygen atoms of the first isocyanate molecule with, respectively, the nitrogen and carbon atoms of the second molecule. The transition state (TS3) involves a low energy barrier of 28.5 kcal mol^{-1}, significantly lower than that implied in the radical initiation with O_2 (around 44 kcal mol^{-1}). The formed intermediate, that lies 3.8 kcal mol^{-1} above CH_3NCO + CH_3NCO, decomposes into CO_2 and N,N'-dimethylcarbodiimide (CH_3NCNCH_3) with an energy barrier of only 22.9 kcal mol^{-1}. The latter species has been experimentally observed by Blake and Ijadi-Maghsoodi[17] during the pyrolysis of methylisocyanate and a similar reactional pathway was proposed to explain its formation, even if no energy barrier was given by these authors. It can be noted that this reaction is slightly exothermic (-2.6 kcal mol^{-1} at 0K). Another possibility involves the addition of the carbon and oxygen atoms of the first molecule with, respectively, the carbon and nitrogen atoms of the second one. However, the energy barrier is very high (94.0 kcal mol^{-1}) and cannot compete with the former pathway. The last bimolecular reaction considered is the cycloaddition between the two carbon and nitrogen atoms respectively. Again, the barrier height is high and this pathway can be neglected.

It is well known that methyl isocyanate can polymerize or form cycles[38]. The cyclotrimerization leads to 1,3,5-trimethyl-1,3,5-triazine-2,4,6-trione (figure 4, black line), which is the most commonly observed basic structure and has been found in significant quantity in the residues of the tank incriminated in the Bhopal accident[38]. Even if this reaction is favored by catalysts (metal salts or bases) and occurs at low temperature in condensed phase, we computed the direct trimerization of methyl isocyanate. The energy barrier was computed at the CBS-QB3 level of theory due to the high number of heavy atoms involved. If the reaction is strongly exothermic (risk of thermal runaway in case of incident), the energy barrier is higher than those involved in the formation of carbodiimide. Moreover, entropic effects strongly disadvantage the trimolecular reaction, which will be negligible under pyrolysis or combustion conditions in the gas-phase.

In conclusion, the easiest cycloaddition involves a reaction between two isocyanate molecules and yields CO_2 and the N,N'-dimethylcarbodiimide. In the mechanism, this reaction has been written by performing a Quasi Steady State Approximmation (QSSA) on the cyclic intermediate leading to the following global reaction:

$$CH_3NCO + CH_3NCO = CH_3NCNCH_3 + CO_2 \qquad (R2)$$

Even in lean conditions, this initiation reaction is expected to be dominant during combustion process and shows the role of the carbodiimide as a precursor (branching agent) for the formation of the first

free radicals. Indeed, at the CCSD(T)/aug-cc-VTQ∞Z//B2PLYP-D3/6-311++G(3df,2pd) level of theory, the dissociation energy of the C-N bond is only 69.1 kcal mol^{-1}. Compared to the lower BDE in isocyanate (91.7 kcal mol^{-1}), the carbodiimide will mainly react by the following initiation:

$$CH_3NCNCH_3 = \bullet CH_3 + \bullet NCNCH_3 \quad (R3)$$

It is worth noting that the reactions $CH_3NCNCH_3 + CH_3NCNCH_3$ and $CH_3NCNCH_3 + CH_3NCO$ can also exist, with a mechanism similar to the reaction going through TS3, but here the products formed are identical to the reactants.

- ***Propagation steps***

As mentioned above, N,N'-dimethylcarbodiimide acts as an branching agent and allows the creation of the first free radicals. Once these radicals are formed, they will be able to react with methyl isocyanate through propagation steps. In this work, several propagations have been considered and the rate coefficients calculated.

• H-abstractions

H-atom abstractions involving H•, $\bullet CH_3$, •OH, •O•, $\bullet NH_2$, $H_2CN\bullet$, $NO_2\bullet$, $CH_3NH\bullet$, $\bullet CH_2NH_2$ and •NCO on CH_3NCO have been taken into account in the mechanism. $H_2CN\bullet$, $CH_3NH\bullet$, $\bullet CH_2NH_2$ and •NCO radicals were selected on the basis of preliminary simulations performed with a test mechanism. For these radicals, unimolecular decompositions are quite difficult and their concentration is high enough to be considered in bimolecular H-atom abstractions. Particular attention was paid to the H-abstraction by •OH radical since it is a sensitive reaction, which involves reactive complexes, as shown in Figure 5.

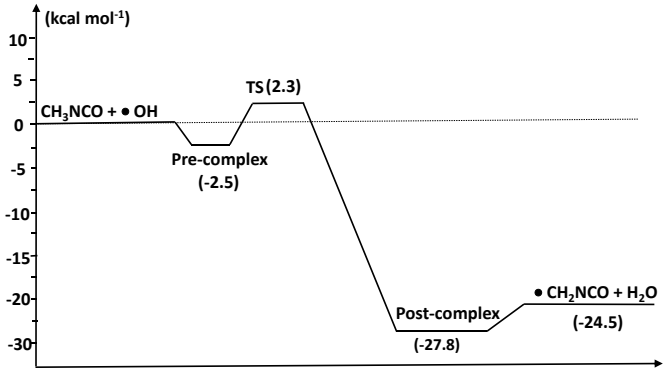

Fig 5. Potential energy profile of the H-atom abstraction by OH. E_{0K+ZPE} are given in kcal mol^{-1}.

This energy profile has been introduced in the MESS code [30] to calculate the corresponding rate coefficients that explicitly take into accounts the van der Waals pre- and post-reactive complexes. The formation of complexes has been treated using the phase space theory as previously detailed for initiation reactions with O_2.

- *Fate of •CH_2NCO*

H-atom abstractions from CH_3NCO yield •CH_2NCO radical, which undergoes N-CO bond scission and leads to the formation of the methylene amidogen radical, CH_2N•, and CO:

$$\bullet CH_2NCO \rightarrow \bullet CH_2N + CO \qquad (R4)$$

The computed rate constant shows a strong dependence with the pressure, as shown in Figure 6.

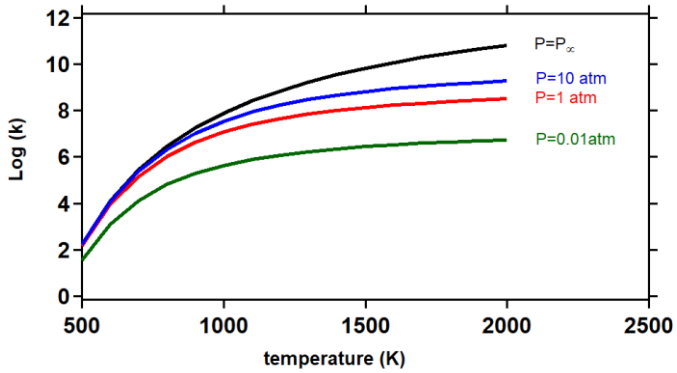

Fig 6. Pressure dependence of the rate constant involved in the β-scission of •CH_2NCO

Rate coefficients have been introduced in the mechanism by considering a double Arrhenius expression in order to correctly represent this effect.

• H-atom additions

Hydrogen addition plays a significant role during pyrolysis or combustion of hydrocarbons. In the case of methyl isocyanate, hydrogen addition can occur on carbon and nitrogen atoms. Figure 7 depicts the energy profile as well as the subsequent reactions of the adducts formed (W_1 and W_2 in figure 7). H-atom additions involved significant energy barriers (around 8 kcal mol^{-1}) compared to those with alkene (usually around 1 or 2 kcal mol^{-1}). The adducts formed are connected *via* 1,2-hydrogen shift with a barrier height of 36 kcal mol^{-1} for the easiest path ($W_2 \rightarrow W_1$). W_1 and W_2 can also isomerize to form a third adduct (W_3) *via* 1,3 and 1,2-hydrogen shift with energy barriers around 35 and 44 kcal mol^{-1}, respectively. All these adducts may react by β or α-scissions but it can be seen that for W_2 and W_3 these reactions involve high-energy barriers. Considering the energy profile in figure 7, we can expect that W_2 will mainly react by the reverse reaction yielding ICM+H and that the products from W_3 will be negligible. In fact, W_1 will be the main adduct and can decompose through two pathways: a β-scission leading to isocyanic acid (HNCO) and an α-scission yielding carbon monoxide. Note that the energies of these exit channels remain under the energy of the entrance channel.

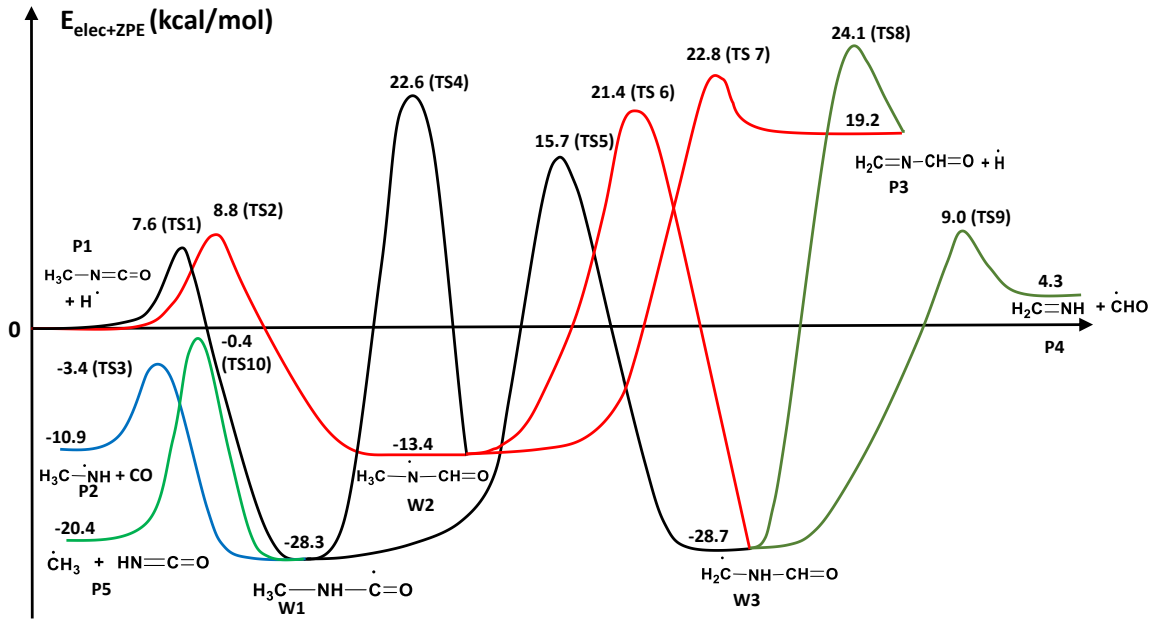

Fig 7. Relative energies involved in H-additions on CH_3NCO, with the subsequent decompositions. E_{0K+ZPE} are given in kcal mol^{-1}.

Pressure dependent rate coefficients were calculated with the MESS code and confirmed that only W_1 is important. Depending on the pressure considered, this adduct can be more or less stabilized. At low pressure, CH_3NCO will directly react with •H to form P_2, while at high pressure the stabilization becomes dominant. In this study, both routes were considered but to avoid introducing W_1 in the mechanism, we performed a quasi-steady state approximation on W_1 and we only wrote the following two reactions:

$$CH_3NCO + H = CO + CH_3NH\bullet \quad (k_1) \qquad (R5)$$

$$CH_3NCO + H = HNCO + \bullet CH_3 \quad (k_2) \qquad (R6)$$

with k_1 and k_2 being the rate constant involving both the formally direct pathway and the stabilization of W_1. Figure 8 shows the branching ratio corresponding to k_1/k_2, as a function of temperature and pressure. At low temperature, the formation of CO is largely preponderant compared to the pathway leading to isocyanic acid. This behavior is more pronounced at high pressure. As the temperature increases, the ratio k_1/k_2 decreases and the flux of CO reaches a value about twice that of isocyanic acid.

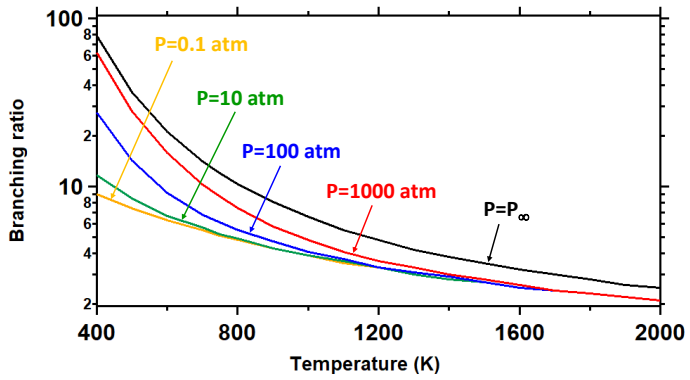

Fig 8. Branching ratio between the rate constant of CO (k_1) and isocyanic acid (k_2) formation as a function of pressure and temperature.

- O-atom addition

Reactions with oxygen atom can play a significant role in the oxidation process at high temperature. In the case of methyl isocyanate, two additions of oxygen (^3O) can be envisaged: a first one on the carbon atom bearing the double bond and a second on the nitrogen atom. Figure 9 illustrates the energy profile corresponding to the two additions and the subsequent reactions.

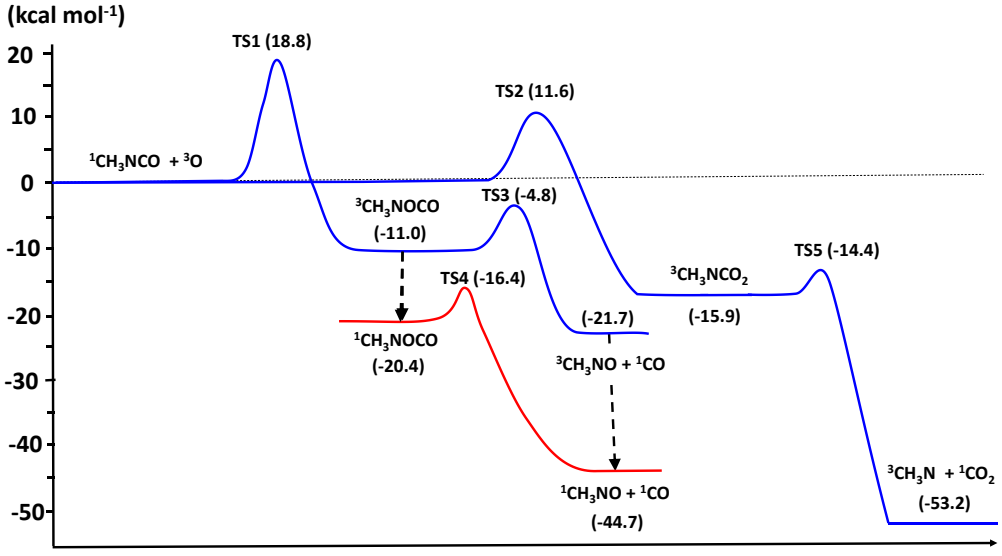

Fig 9. Energy profile of the addition of ^3O on methyl-isocyanate. Blue curve: triplet surface. Red curve: singlet surface

The addition of ^3O on the nitrogen and carbon atom involves energy barriers, at 0K, equal to 18.8 and 11.6 kcal/mol respectively. It is worth noting that these barriers are higher than those encountered for similar reactions with hydrocarbons such as alkenes. The T_1 diagnostic for these two reactions is close to 0.03, which gives correct confidence in the method used to perform the calculations. Several reactions for the adducts formed (CH_3NOCO and CH_3NCO_2) were investigated but only the easiest pathways for each structure are shown in Figure 9. The reaction of CH_3NCO_2 involves a bond breaking between the nitrogen and carbon atom and yields to the formation of carbon dioxide and a triplet

radical CH_3N. The barrier height is low and the reaction is strongly exothermic with an enthalpy of reaction close to -53 kcal/mol at 0K. The second reaction also involves a bond scission to form carbon monoxide and nitrosomethane CH_3NO. The two products are in the singlet state and their formation require inter system crossing (ISC) to occur. A correct treatment of such electronic state changes is not straightforward and is beyond the scope of this study. However, it can be seen that the energies involved in the reactions of the adducts are always below the entry channel. Under these conditions, the two reactions will be kinetically controlled by the first step, *i.e.*, the addition of ^3O. Thus, the two following reactions have been considered in the mechanism:

$$CH_3NCO + {}^3O = {}^3CH_3N + CO_2 \quad (R7)$$

$$CH_3NCO + {}^3O = CH_3NO + CO \quad (R8)$$

with rate constants linked to TS_1 and TS_2 respectively.

- O_2-addition

The last propagation step considered is the addition of the CH_2NCO radical on oxygen molecule. For hydrocarbons, the addition of radicals on O_2 represents an important process in the low or medium temperature range. In this study, we only considered the first O_2-addition with two possible reaction pathways involving the addition on the two carbon atoms (Figure 10).

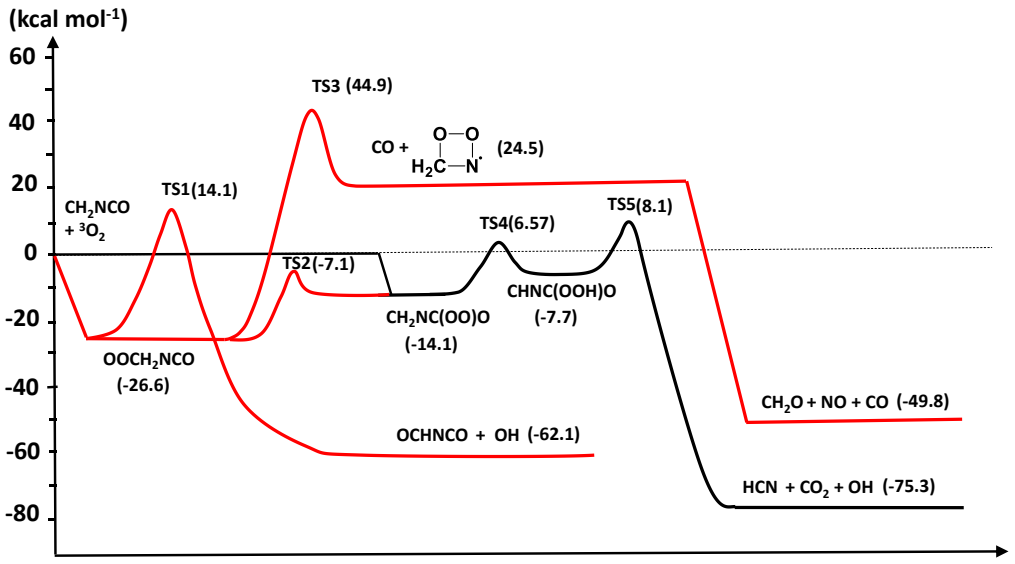

Fig 10. Reactions of CH_2NCO with $^{(3)}O_2$. Detailed pathways with the relative energies (0K) given in kcal mol^{-1}.

Additions to O_2 are barrierless and an accurate calculation of the rate constants remains challenging. In this study, the rate coefficients were chosen from reference[39] and related to the addition of n-C_4H_9 on O_2. The addition of O_2 to the CH_2 group leads to a more stable peroxyl radical ($OOCH_2NCO$) than that resulting from the addition to the carbonyl group ($CH_2NC(OO)O$). Two low energy pathways are related to the former peroxyl radical. The first one involves an 1,3-hydrogen shift (TS_1) to form

HOOCHNCO, which is not stable and directly decomposes into OH and OCHNCO in accordance with the Intrinsic Reaction Coordinate (IRC) calculation. The second pathway involves an O_2-transfer (TS_2) and permits to connect the two peroxyl radicals together with a low energy barrier (19.5 Kcal mol^{-1}). A third decomposition pathway of $OOCH_2NCO$ involves a cyclisation with the nitrogen atom and a direct CO elimination (TS_3), but with a prohibitive energy barrier close to 71 kcal mol^{-1}. At the level of theory considered in this study, no transition state was found for the decomposition of the cycle formed, and we directly considered the formation of CH_2O, NO and CO. The second peroxyl radical, $CH_2NC(OO)O$, can undergo an 1,5-hydrogen shift (TS_4) to form CHNC(OOH)O, which in turn decomposes into CO_2, HCN and OH with an energy barrier of 15.8 kcal mol^{-1} (TS_5).

3.1.2 Reactions of the primary products

The primary mechanism describes the main consumption pathways of methyl isocyanate. Most of the primary products are included in the mechanism developed by Glarborg et al.[32] to model nitrogen chemistry, which was therefore added to the primary reactions of MIC as a reaction base. However, the decomposition of N,N'-dimethylcarbodiimide (CH_3NCNCH_3), a key product in the decomposition of isocyanate, was missing. Indeed, we previously saw that the most likely unimolecular decomposition of methyl isocyanate yields CH_3NCNCH_3 by a concerted reaction. Moreover, the bond dissociation energy of the methyl group is equal to 69 kcal mol^{-1}, a value much lower than the BDE involved in ICM (91.7 kcal mol^{-1}). In these conditions, the N,N'-dimethylcarbodiimide will act as a degenerate branching agent. Even if the quantities formed will be low (based on the experiments of Blake et al.[17]), it will create the first free radicals, which will mainly react on the MIC to promote the radical chain mechanism. In this study, we investigated the consumption pathways of CH_3NCNCH_3, but we only kept the main reactions in order to reduce the mechanism as much as possible.

- ***Initiation reactions of CH_3NCNCH_3***

As for methyl isocyanate, the unimolecular initiations are written in the reverse direction (termination). For the C-H bond breaking, we used a correlation from EXGAS software[36], while for the methyl group cleavage we retained a value equal to 10^{12} cm^3 mol^{-1} s^{-1}, close to that proposed by Faravelli et al.[40] or Davis et al. [41] for the combination of $\bullet CH_3$ and $\bullet CHCCH_2$ radicals (formation of 1,2-butadiene). This unimolecular initiation leads to formation of $\bullet CH_3$ and $CH_3NCN\bullet$ (R3). For the latter radical, we considered the terminations with H-atoms as well as disproportionations with small radicals. The rate constants are based on analogies with similar reactions proposed by Tsang for allyl radical $\bullet C_3H_5$ [42].

Due to the unsaturated structure of the carbodiimide, several concerted reactions can be envisaged. The figure 11 depicts the different channels investigated.

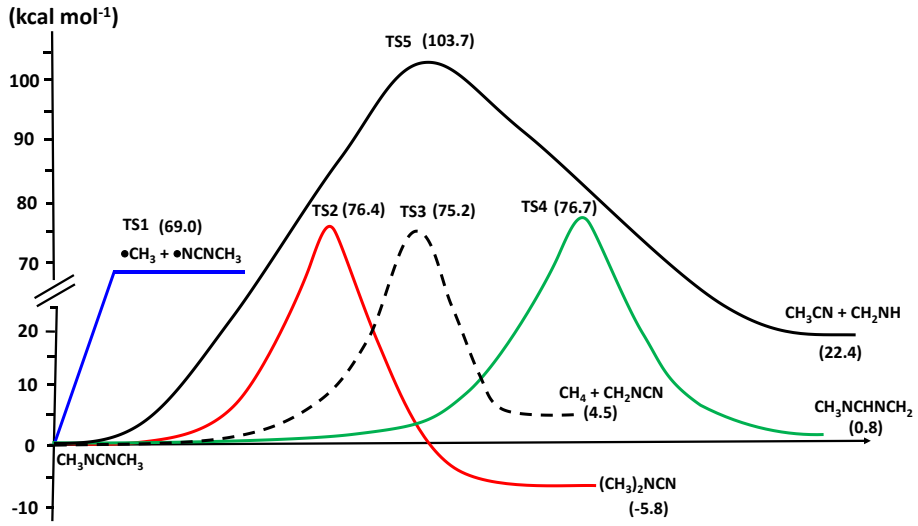

Fig 11. Energy profile for the unimolecular initiation of CH_3NCNCH_3. Energies at 0K are given in kcal mol^{-1}.

All of these reactions need higher energy barriers than the dissociation energy involved in the CH_3 bond of the carbodiimide. In particular, the transition state corresponding to the transfer of methyl (TS2) has an energy barrier of 7 kcal mol^{-1} higher than the N-C bond breaking, despite the formation of dimethylcyanamide, a more stable product than the reactant (-5.8 kcal mol^{-1}). In the same way, the H-transfer leading to $CH_3NCHNCH_2$ (TS4) or the six-centered concerted reaction yielding to CH_2NCN and methane (TS3) cannot compete with the radical initiation. Moreover, this latter reaction has a very poor T_1 diagnostic (0.05) which clearly shows a multireference character. The last bimolecular initiation investigated is the reaction between CH_3NCNCH_3 and O_2 and we took into account the formation of pre- and post-reactive complexes to determine the value of the rate constant, using the same approach as for CH_3NCO+O_2.

- ***Propagation steps***

Due to the low dissociation energy of the N-CH_3 bond, *N,N'*-dimethylcarbodiimide is expected to easily react *via* unimolecular initiation. However, propagation steps cannot be neglected *a priori*. The rate constants of the H-atom abstractions by H•, •CH_3, •OH, •O•, •NH_2, CH_3NH• and •CH_2NH_2 radicals have been computed at the same level of theory as those for CH_3NCO. H-atom abstractions yield CH_3NCNCH_2• radical, which can decomposes by β-scission with a barrier height of 30.6 kcal mol^{-1}:

$$CH_3NCNCH_2\bullet = CH_2NCN + CH_3\bullet \qquad \text{(R9)}$$

As for •CH_2NCO, we took into account the pressure effect and we expressed the rate constant with a double Arrhenius expression.

H-atom additions were also included in the mechanism and can occur on the carbon atom bearing the double bond or the nitrogen atoms. Due to the symmetry of dimethylcarbodiimide, only

two additions must be considered. Figure 12 shows the energy profile involved in the H-atom addition on CH_3NCNCH_3 and the subsequent β-scissions or H-shifts.

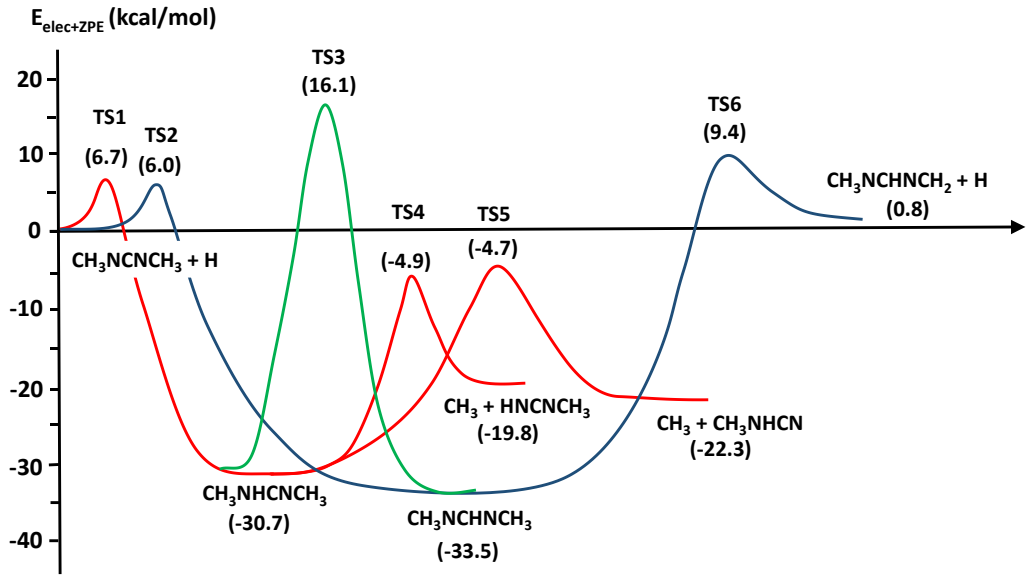

Fig 12. Energy profile of the H-additions on N,N'-dimethylcarbodiimide and the subsequent β-scissions of adducts formed. Energies at 0K are given in kcal mol^{-1}.

As shown in Figure 12, the additions of H-atom to carbon and nitrogen atoms involve similar energy barriers (6.7 and 6.0 kcal mol^{-1}) and have close enthalpies of reaction at 0K. However, the exit channel for $CH_3NCHNCH_3$ (TS_6) requires an energy barrier that lies above the entrance energy channel and is higher than those involved in the β-scission of $CH_3NHCNCH_3$ (TS_4 and TS_5). For $CH_3NHCNCH_3$, the computed rate constant of the β-scission leading to methylcyanamide (CH_3NHCN) and $\bullet CH_3$ is always, at least, 3.5 times higher than that involved in the formation of *N*-methylcarbodiimide ($HNCNCH_3$) and $\bullet CH_3$. The difference is mainly explained by the hindrance of two internal rotations in TS_4 against only one in TS_5, which reduces the entropy of the former more significantly. As previously mentioned, CH_3NCNCH_3 acts as an inducer for the overall reaction but the quantity formed will remain small and will have a limited impact on the amounts of products formed during the combustion or pyrolysis of ICM. Therefore, we simplified the hydrogen addition pathways by only considering the addition on nitrogen atom with the formation of $CH_3NHCN + \bullet CH_3$ as the sole exit channel.

The last propagation step considered for the *N,N'*-dimethylcarbodiimide is the oxygen-atom addition (^3O). The two possible additions require notably different energy barriers. At the B3PLYP-D3/6-311++G(3df,2pd) level of theory, the addition on the nitrogen atom involves an energy close to 13 kcal/mol against 5 kcal/mol for the addition on the carbon-atom. The adduct formed for the latter addition is 46.6 kcal/mol below the entrance energy of the reactants and can easily decompose into ICM and CH_3N, with a barrier height of only 12.3 kcal/mol, *i.e.* 34.3 kcal/mol below the entrance

channel. In order to reduce the size of the mechanism as much as possible, we only considered this single reaction pathway and we used the addition rate constant as overall rate constant (figure 13):

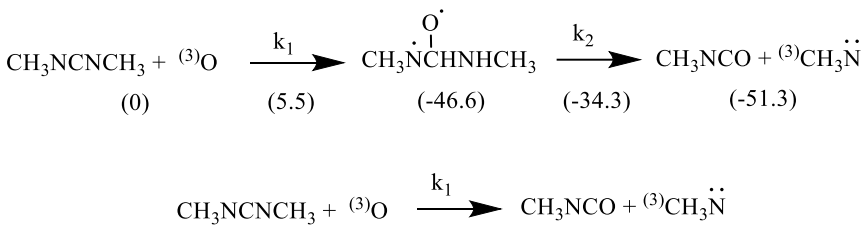

Fig 13. Reactions of $^{(3)}O$ with N,N'-dimethylcarbodiimide. (a) Detailed pathways with the relative energies (0K) given in kcal/mol at the B2PLYP-D3/6-311++G(3df,2pd) level of theory. (b) Global reaction taken into account in the mechanism.

3.1.3 Reactions of the secondary products

At this stage of the mechanism generation, two secondary products are formed whose decomposition reactions are not included in the reaction base [1]. These two molecular products are methylidenecyanamide (CH_2NCN) and methylcyanamide (CH_3NHCN). Reaction classes similar to those described above have been applied to these two species and have been included in the final mechanism. Thus, unimolecular and bimolecular initiations (with O_2) were considered. The formation of pre- and post-reactive complexes has a significant effect on the rate constant, in the case of CH_2NCN+O_2. Without considering the reactive complexes, the rate constant would be higher by a factor ranging from 7 to 4.5 between 500 and 2000K respectively. This result can be explained by the formation of highly stabilized complexes, especially for the post-complex which is 7 kcal mol^{-1} lower than the exit channel ($CHNCN+HO_2$). For H-atom abstractions, only the reactions involving •H, •OH, •O• and •CH_3 radicals have been taken into account due to their significant role in pyrolysis or combustion. H-atom additions and the subsequent reactions (H-shift, β or α-scission) have been also considered as presented in Figure 14 forCH_2NCN.

The full potential energy surface has been introduced in the MESS code of the PAPR suite[30] to take into account pressure effect and identify the most important pathways. From this analysis, two channels have been retained. The first one involves H-addition on the carbon atom of the cyano group *via* TS_3 (green line, in Figure 14). Even at high pressure the CH_2NCHN adduct is not stabilized and directly decomposes into CH_2N• and HCN. Thus, only the following reaction was considered in the mechanism:

$$CH_2NCN+H=CH_2N\bullet+HCN \qquad (R10)$$

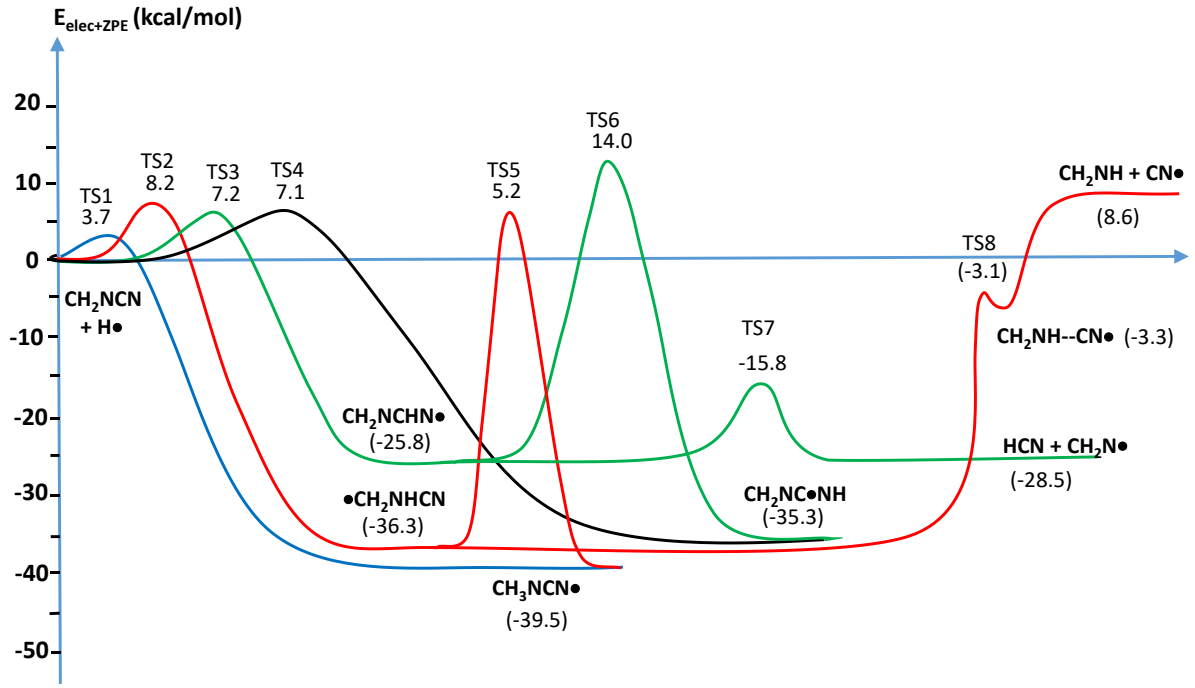

Fig 14. Energy profile of the H-additions on CH_2NCN with the subsequent β and α-scissions of the adducts formed. Energies at 0K are given in kcal mol^{-1}.

The second pathway involves the H-atom addition on the $–CH_2$ group (TS1). This addition leads to the formation of $CH_3NCN•$ and has the lowest energy barrier (blue pathway on Figure 14). However, the exit channel requires an 1,2-H-shift, leading to CH_2NHCN, followed by a β-scission to form methanimine (CH_2NH) and •CN. Note that an intermediate complex was found at the B2PLYP-D3 level of theory and was considered in the calculation performed with the MESS code. Depending on the pressure, the stabilization of the wells can be significant and the reactions introduced in the mechanism contain both the formally direct pathway and the formation of adducts.

Only the H-addition on the carbon atom of CH_3NHCN has been considered in the mechanism since it involves a lower energy barrier than the addition on the nitrogen atom. Moreover, the β-scission of the adduct formed is easier in the former case (about 10 kcal mol^{-1} lower).

We also considered O-atom additions for these two secondary products. For CH_2NCN, only additions on the carbon atoms were retained because the energy barriers are much lower than those for additions on nitrogen atoms (respectively 3.6 and 6.1 versus 13.4 and 16.3 kcal mol^{-1} at the B2PLYP-D3 level of theory). Several decomposition pathways were investigated and we selected those with energy barriers below the entrance channel. We also considered the first reaction (O-addition) as the limiting step to deduce the rate constant and globalize the reaction as follows:

$$CH_2NCN+{}^3O=CH_2O+NCN \qquad (R11)$$

$$CH_2NCN + {}^3O = H_2CN\bullet + \bullet NCO \quad (R12)$$

In the same way, the O-addition on the carbon atom of CH_3NHCN leads to the following products:

$$CH_3NHCN + {}^3O = CH_3NH\bullet + \bullet NCO \quad (R13)$$

3.1.4 Update of the reaction base for small nitrogen compounds

Few reactions have been added to the reaction base developed by Glaborg et al.[1] or updated to improve the accuracy of the thermal decomposition mechanism of MIC. Disproportionations and combinations involving $H_2CN\bullet$, $CH_3NH\bullet$, $\bullet CH_2NH_2$, $\bullet NO_2$ and $\bullet NH_2$ were added to the mechanism. The choice of these radicals was based on preliminary simulations, which showed that their concentration was high enough to be considered in such reactions. Particular attention was paid for $H_2CN\bullet$ and $HC\bullet NH$, which are the main precursor of HCN, a major product formed during the pyrolysis of MIC. We considered the β-scission of these two radicals and we deduced rate coefficients from RRKM-ME. Figure 15 shows the comparison between the rate constants obtained and those included in the current reaction base and proposed by Dean and Bozzelli from QRRK calculations [43].

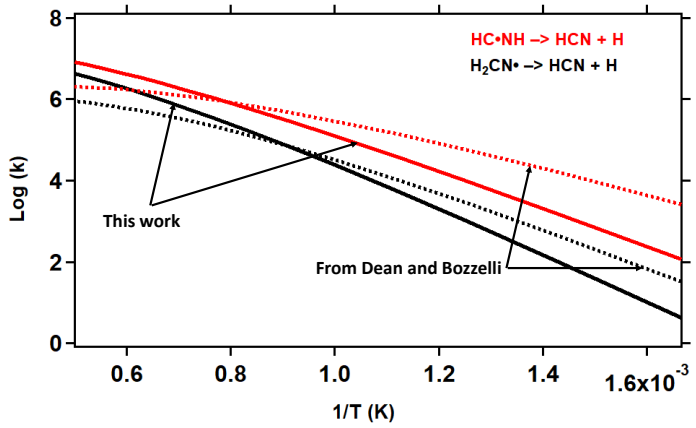

Fig 15. Rate constants of the reactions $H_2CN\bullet \rightarrow$ HCN + H (black) and $HC\bullet NH \rightarrow$ HCN + H (red), at P=0.1 bar, from Dean and Bozzelli[43] and from this work.

Differences are observed, both at low and high temperatures. For $H_2CN\bullet$, the value proposed by Dean and Bozzelli is about 7 times higher than that resulting from our calculation at 600K, while at 2000K the trend is reversed by a factor of 5. A similar evolution is observed for the β-scission of $HC\bullet NH$ but with a higher deviation observed at low temperature (factor 20 at 600K and P=0.1 bar).

H-atom abstractions on CH_2NH and CH_3NH_2 were also updated. These two compounds are products of the decomposition of MIC and the H-atom abstractions by H-atoms are important in pyrolysis. Eventually, the elaborated mechanisms contain a total of 130 reactions, which have been merged with the updated reaction base developed by Glarborg et al. [1] for nitrogen-containing

species. The overall mechanism, as well as the thermodynamic data, are available in the supplemental material.

3.2 Simulations

3.2.1 Pyrolysis of methyl isocyanate.

As previously mentioned, very few studies have been carried out on the thermal decomposition of isocyanates. From the best of our knowledge, the experimental study of Blake and Ijadi-Maghsoodi[17] is the only one on methyl-isocyanate presenting species profiles. Pyrolysis experiments were performed in a closed reactor for temperatures ranging from 700 to 821 K and pressures from 55 to 300 Torr. Blake and Ijadi-Maghsoodi only give the distribution of species for a temperature of 799K and an initial pressure of 150 torr. This experiment was simulated using the Chemkin Pro software with an isothermal batch reactor model. The results obtained are shown in Figure 16.

Overall, the results obtained are in good agreement with the experimental data. The increase in total pressure (ΔP) is well reproduced by the model, as shown in Figure 16a (experimental data are only given for short residence times). This result confirms that the model is able to capture the overall reactivity of the pyrolysis of methyl isocyanate. The product partial pressures vs. time up to 130 min are presented in figure 16 (b)-(f). Concerning major species, the model correctly reproduces CO and H_2. Figure 17 depicts the reaction flow analysis for a conversion of CH_3NCO equal to 50%. CO is mainly formed by H-abstraction on methyl-isocyanate, followed by an α-scission of the CH_2NCO radical (45.6%). It is also formed by H-atom addition on the nitrogen atom of ICM, followed by a β- or α-scission. H-abstraction by H-atom is largely preponderant (about 75% of the global consumption flux) and overall leads to a large amount of dihydrogen, H_2.

The simulations show a significant deviation from the raw experimental data with respect to HCN formation and MIC consumption (circles in Figures 16e and 16f). These results are not consistent with the rest of the simulations, which are in agreement with the experiments. In fact, Blake and Ijadi-Maghsoodi [17] put forward an experimental problem related to the analytical part. At the end of the reaction, the products (and the unconsumed reactant) are recovered in a cold trap but a reaction occurs between HCN and MIC in this trap, leading to the formation of a new product. This problem was confirmed by the authors, who performed specific experiments where HCN and ICM were mixed at 723K [17].

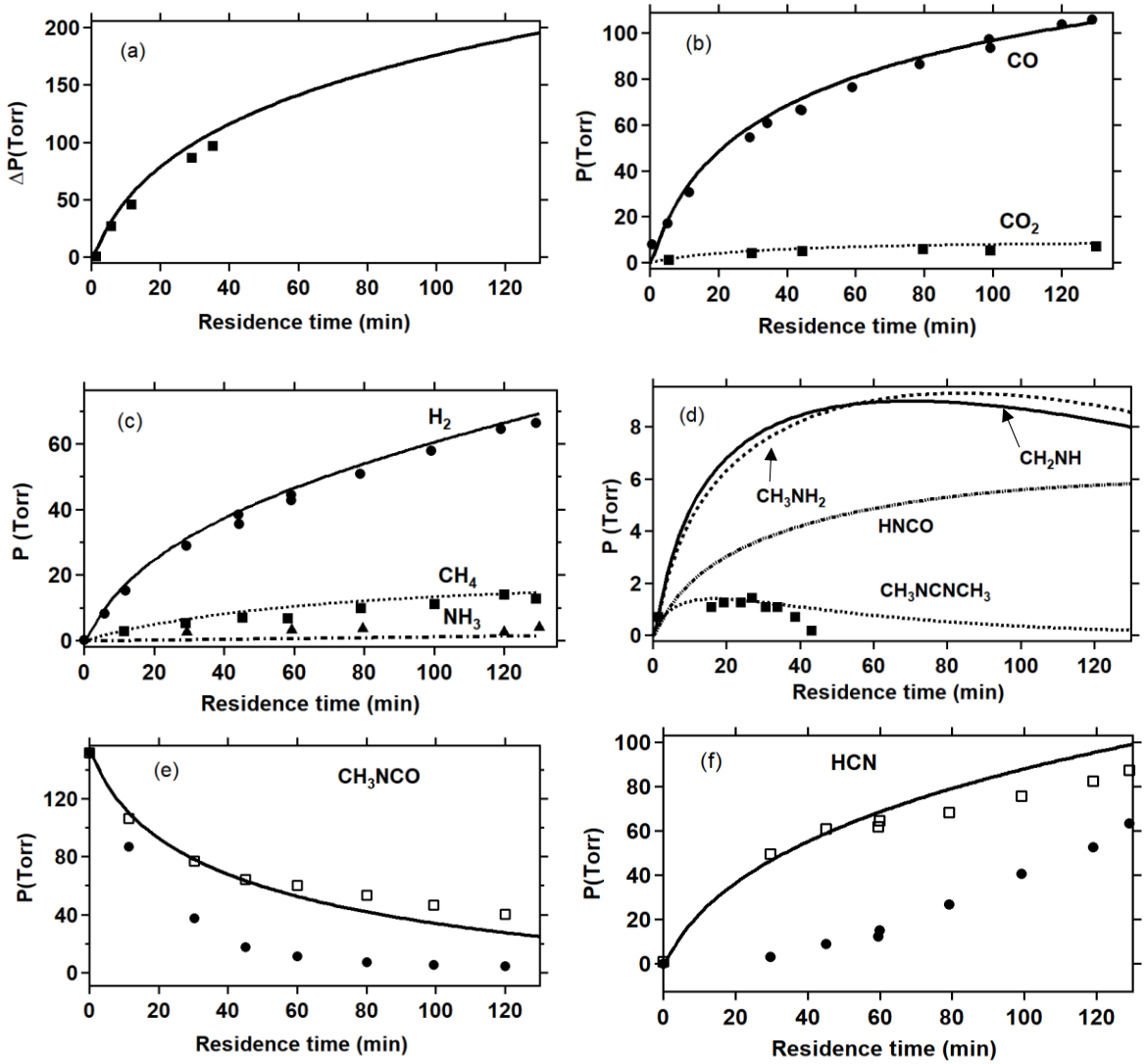

Fig 16. Comparison between experiments from [17] (points) and simulations from the model developed in this study (lines). Circles in Figures (e) and (f) correspond to original experimental data of Blake and Ijadi-Maghsoodi[17], while the open squares correspond to corrected experimental values (see text).

At this temperature, no reaction occurs in the reaction vessel but appears in the analytical section of the apparatus. In order to take into account this effect, we sought to rationalize the experimental data. To "correct" the experimental data of methyl isocyanate, we fitted the experimental HCN profiles using a polynomial regression in order to obtain a continuous function representing its concentration as a function of time. Next, we calculated the difference between the simulated values of HCN and those obtained from the experimental polynomial. We assumed that this difference was mainly due to the HCN fraction reacting with the MIC in the trap and we added this difference to the experimental MIC values. These "corrected data" are represented by open squares in Figure 16e.

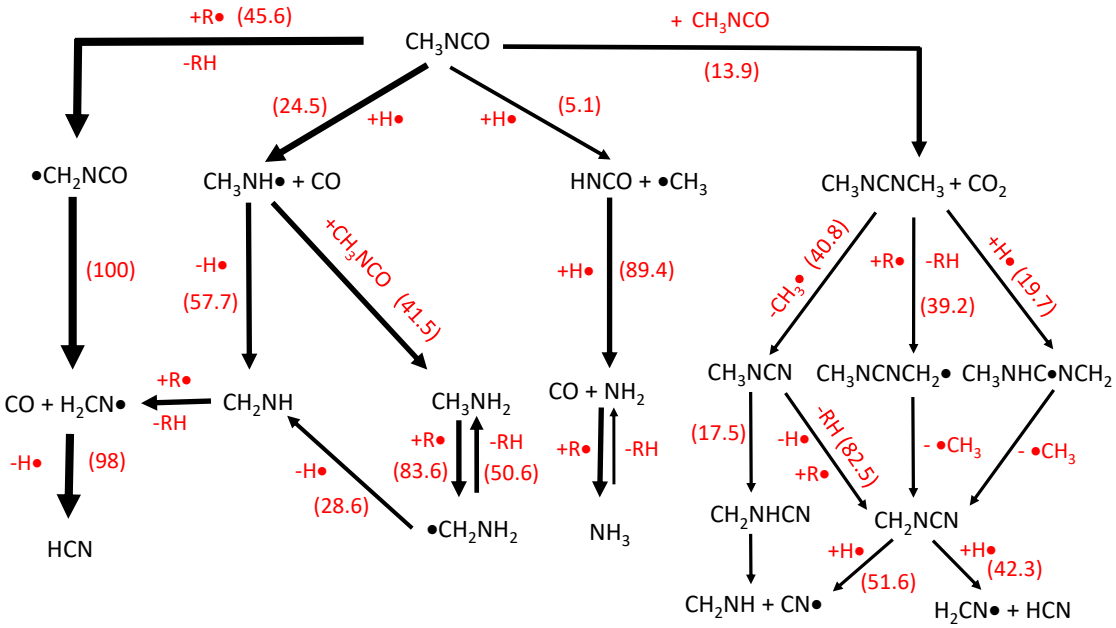

Fig 17. Reaction flow analysis under pyrolysis conditions, for a conversion of methyl isocyanate equal to 50%. T=799 K, P=150 torr.

We performed the same procedure to modify the experimental data of HCN, assuming that the difference between the experimental and simulated amounts of MIC corresponded to the fraction reacting with HCN. Even if this approach can be questionable, Figures 16e and 16f show a clear improvement and a good consistency between experimental and simulated data, both for CH_3NCO and HCN (squares and curves in Figures 16e and 16f).

CO, HCN and H_2 are the main products of the MIC pyrolysis and their formation can be mostly explained by the propagation step showed in Figure 18.

$$CH_3NCO + \bullet H \rightarrow \bullet CH_2NCO + H_2 \quad (1)$$

$$\bullet CH_2NCO \rightarrow H_2CN\bullet + CO \quad (2)$$

$$H_2CN\bullet \rightarrow HCN + \bullet H \quad (3)$$

$$CH_3NCO = HCN + CO + H_2 \quad (4)$$

Fig 18. Main propagation step involved in the pyrolysis of CH_3NCO.

Carbon monoxide is also produced from the addition of hydrogen atom to CH_3NCO. Similarly, HCN is formed from the decomposition of N,N'-dimethylcarbodiimide, and to a lesser extent from H-addition. Although the corresponding fluxes are lower, they explain the higher amount of CO and HCN observed compared to H_2 (Figures 16b, 16c and 16f). The good agreement between simulations and experimental results shows that the branching ratio between the different reaction pathways is well modeled by the mechanism.

Among minor products, carbon dioxide (Figure 16b) is correctly described by the model, supporting its formation by the proposed pericyclic reaction. Similarly, the mole fraction of CH_3NCNCH_3

is consistent with the experimental data (Figure 16d) even though the quantities formed are small. Reaction flow analysis (Figure 17) shows that carbodiimide is mainly consumed by unimolecular initiation (40.8%), H-atom abstraction (39.2%) and H-atom addition (19.7%). The correct agreement obtained by simulation allows a good confidence in the rate constants proposed.

Methane is also a minor product formed by H-atom abstraction by CH_3 and Figure 16c shows that the model correctly reproduces its formation. CH_3 is mainly produced by H-atom addition on CH_3NCO (42%) or CH_3NCNCH_3 (11%), followed by α- or β-scission. Other sources of methyl radicals come from the unimolecular initiation of CH_3NCNCH_3 (17%) and the β-scission of CH_2NCNCH_3 (20%).

NH_3 is the last minor product experimentally measured with a maximum partial pressure equal to 4 torr. Our model underestimate the formation of ammoniac by a factor close to 2.5. Reaction flow analysis shows that NH_2 (the precursor of NH_3) is mainly formed by H-addition on HNCO followed by α-scission. This reaction has been recalculated but the rate constant obtained doesn't differ significantly from the value proposed by Baulch et al.[44]. The H-abstraction between NH_2 and HCN has been also added to the mechanism but this reaction acts in the reverse direction.

Finally, we added profiles of products not mentioned by Blake and Ijadi-Maghsoodi[17] but appearing in the simulations at significant partial pressures (Figure 16d). These species are methylamine (CH_3NH_2), isocyanic acid (HNCO) and methanimine (CH_2NH). Blake and Ijadi-Maghsoodi give mass balances between 96 and 100% for oxygen atom against 80 to 90% for hydrogen and carbon atoms and only 70% for nitrogen atom. The prediction by the model of species not observed experimentally and containing mainly carbon, hydrogen and nitrogen atoms is then not inconsistent with the given mass balances.

A sensitivity analysis was also performed for the conversion of MIC and the results are given in Figure 19.

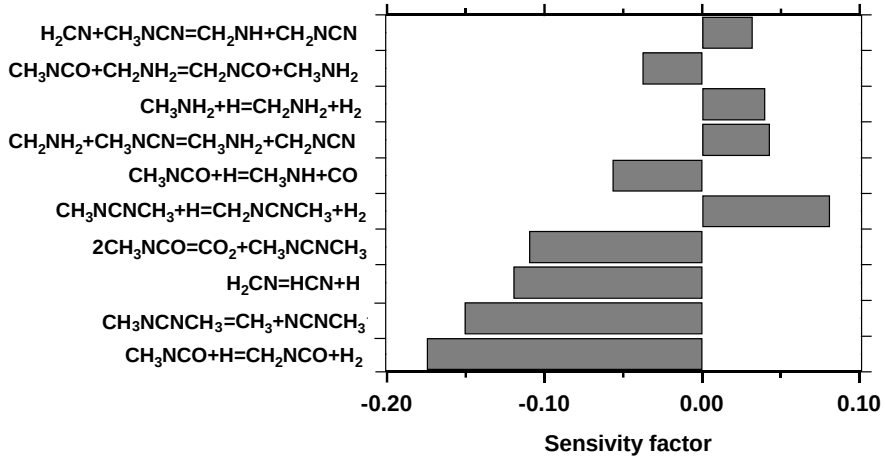

Fig 19. Sensitivity analysis related to the pyrolysis of CH_3NCO and for a conversion equal to 50%. T=801 K, P=150 Torr.

As expected, the reactions having the most promoting effect on the consumption of MIC are the H-abstractions by H-atom. Among the most sensitive reactions, two involved the formation and consumption of N,N'-dimethylcarbodiimide: the pericyclic reaction leading to the formation of CO_2 and the unimolecular initiation of CH_3NCNCH_3. As already mentioned, CH_3NCNCH_3 plays the role of branching agent producing free radicals. At 50% of conversion, these reactions still play a significant role due to the low value of the bond dissociation energy of CH_3-----$NCNCH_3$ and, *a contrario*, rather high energy barriers involved in propagation steps. Another reaction having a significant promoting effect is the β-scission of $H_2CN\bullet$ yielding to HCN and H-atom. Indeed, this reaction is the limiting step in the main propagation loop (Figure 18). At 0K, the energy barrier of the $H_2CN\bullet$ radical is close to 36 kcal mol^{-1} against 24.2 for the α-scission of CH_2NCO. Moreover, these two reactions are strongly pressure dependent, especially for the β-scission of $H_2CN\bullet$. Reactions having an inhibiting effect act on the consumption or production of H-atoms. Indeed, H-abstractions by H-atom on primary products ($CH_3NCHNCH_3$, CH_3NH_2) compete with the H-abstraction on the reactant and inhibit its consumption. In the same way, H-abstractions by $H_2CN\bullet$ or CH_2NH_2 on CH_3NCN prevent β-scission of these radicals to form reactive H-atom.

3.2.2 Combustion of methyl isocyanate

To the best of our knowledge, no kinetic study nor speciation is available in the literature for methyl isocyanate combustion. In order to evaluate our mechanism under oxidation conditions, we simulated the auto-ignition temperature (T_{ign}) of methyl-isocyanate given in the literature, which is equal to 807K [45, 46]. This temperature has been experimentally obtained from the standard ASTME659-78 test for liquid chemicals[47]. The simulations were performed in a closed reactor with a volume equal to 500 cm^3 and a heat loss transfer coefficient of 19 W m^2 K^{-1} [48, 49]. To obtain T_{ign}, an iterative procedure was applied by gradually increasing the temperature, until the pressure peak was reached at a reaction time equal to 10 minutes. Note that this simple 0D model does not correctly capture the convective heat and mass transfers in the apparatus during real experiments.

Eventually, a value of T_{ign} equal to 789K was obtained (Figure 20). Given the uncertainties inherent to this type of calculation, this result remains in agreement with the experimental value, which is only 18K higher.

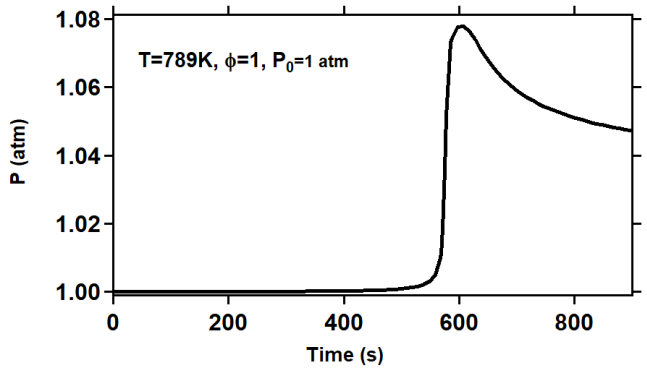

Fig 20. Simulation of the pressure-time profile during the combustion of CH_3NCO in a closed vessel, at P_{init}=1atm, T_0=789K and ϕ = 1

Reaction flux and sensitivity analyses (Figures 21 and 22) were performed using Chemkin pro for a conversion of 30% and a temperature equal to 800K, *i.e.* for parameters corresponding to the pressure peak presented in Figure 20.

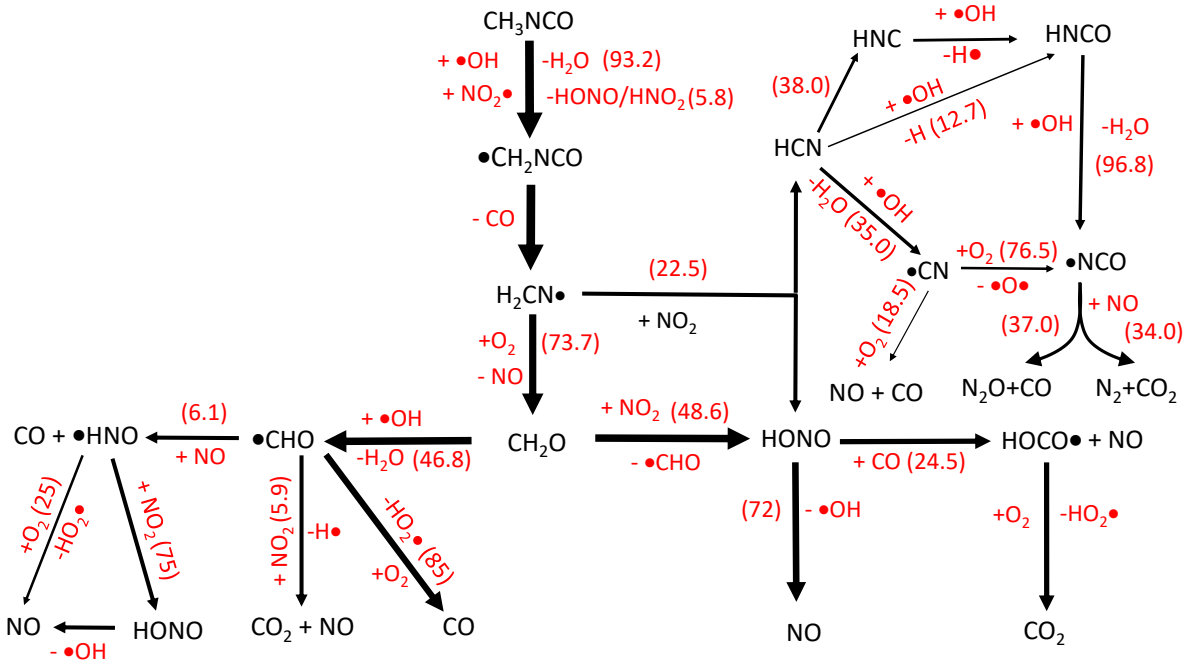

Fig 21. Reaction flow analysis related to CH_3NCO combustion and for a conversion equal to 30%. φ =1, T=800 K, P=1atm.

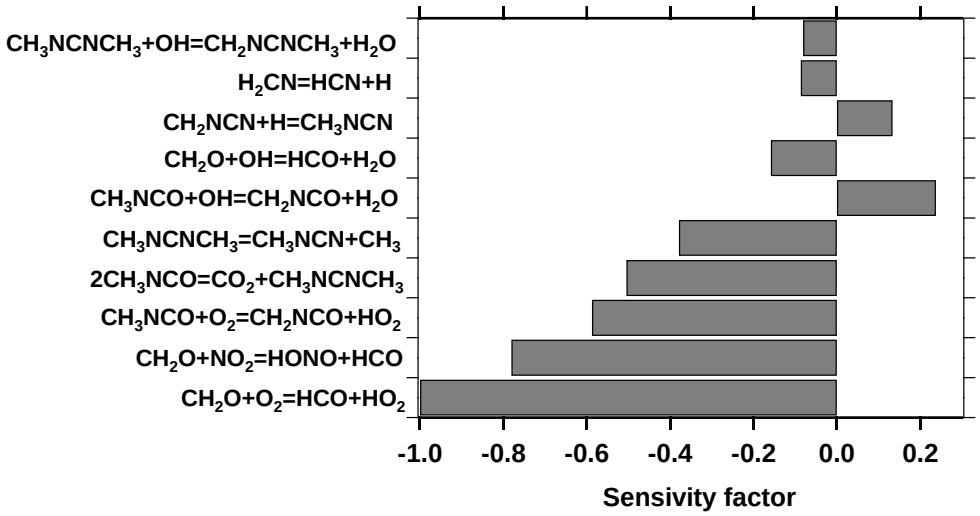

Fig 22. Sensitivity analysis related to the combustion of CH_3NCO and for a conversion equal to 30%. Φ=1, T=800 K, P=1atm.

Under these conditions, methyl isocyanate is mainly consumed by H-abstraction by OH to form CH_2NCO, which undergoes α-scission to give CO and $H_2CN\bullet$. Most of the latter radical (73.7%) is oxidized by O_2, yielding formaldehyde and nitrogen monoxide. CH_2O reacts by H-abstraction with OH and NO_2. CHO radical is mainly consumed by O_2 and to a lesser extent by reactions with NO or NO_2 to form carbon monoxide or dioxide. On the other hand, nitrous acid (HONO), formed by the reaction between formaldehyde and NO_2, mainly reacts by unimolecular initiation (72%) yielding to OH and NO and in a lesser extend with CO and O_2 (24.5%) to form HO_2, CO_2 and NO.

Figure 21 shows that a small part of $H_2CN\bullet$ reacts by disproportionation with NO_2 leading to the formation of nitrous acid and hydrogen cyanide. This latter compound can isomerize to form hydrogen isocyanide HNC (38%) or react by H-abstraction with OH (35%). In both cases, the reaction pathways mainly yield NCO radical, which reacts with O_2 to form CO or CO_2 and nitrous oxide (N_2O) or N_2.

Figure 22 shows that the two most sensitive reactions are related to the formaldehyde sub-mechanism. Indeed, the bimolecular initiation with O_2 has a promoting effect on the conversion of methyl isocyanate. Similarly, the reaction with NO_2 leads to the formation of nitrous acid, which in turn, mainly reacts by unimolecular initiation, leading to the formation of the very reactive OH radical and NO. Two other sensitive reactions are directly linked with the reactions of MIC. The first involves the bimolecular initiation of methyl isocyanate with an oxygen molecule. This reaction produces HO_2 and CH_2NCO, which decomposes by α-scission to form $H_2CN\bullet$, the main radical involved in the propagation step. The second reaction is related to the formation of the N,N dimethyl-carbodiimide, which acts as branching agent for the MIC conversion (promoting effect). As already mentioned, this compound can easily decompose into CH_3 and CH_3NCN, which subsequently decomposes by β-scission

to release a H-atom. The importance of this last pathway is also highlighted by the sensitivity analysis. It can be noted that other reactions involving the mechanism developed in this study show significant sensitivity coefficients such as H-atom abstractions by OH radical (Figure 22). It can be noted that the additions of CH_2NCO on O_2 have no real impact. In fact, the addition occurs at very short time but the exit channels are not favorable and the peroxyl radicals essentially react by reverse reactions, given back CH_2NCO and O_2.

4. Conclusions

This study focused on the development of the first detailed mechanism for the combustion of methyl isocyanate. Potential energy profiles were obtained on the basis of electronic structure calculations. Pressure dependence and influence of pre-reactant complexes were considered by means of RRKM-ME and phase space theory. The mechanism developed includes 130 reactions, 90 of which have been obtained from electronic structure calculations. This mechanism has been merged with the reaction base developed by Glarborg et al.[1] for small nitrogen containing-species. Simulations were performed to confront the model with experimental results. Overall, a good agreement was obtained for all experimentally quantified species. The flow rate and sensitivity analyses revealed the crucial role played by N,N-dimethylcarbodiimide. This compounds acts as a branching agent due to the low bond dissociation energy between the carbon and nitrogen atoms. Once the first radicals are created, the main propagation loop involves the H-abstraction by H-atom on methyl isocyanate, followed by α- and β-scissions and leads to the formation of HCN, H_2 and CO as major products. H-addition to methylisocyanate also contributes to its consumption. Combustion simulations were focused on the estimation of the auto-ignition temperature (T_{ign}). The model led to a value of T_{ign} consistent with literature data. Under these conditions, methyl isocyanate is mainly consumed by the OH radical and to a lesser extent by NO_2. The decomposition pathway of the radical formed is identical to that observed in the pyrolysis of MIC, with the formation of CO and $H_2CN\bullet$ radical. While $H_2CN\bullet$ mainly decomposes by β-scission ($H_2CN\bullet \rightarrow HCN + H\bullet$) in pyrolysis, under oxidative conditions it mostly reacts with O_2 to give NO and formaldehyde. Sensitivity analysis highlighted the importance of reactions associated with primary and secondary mechanisms, such as unimolecular and bimolecular initiations with O_2 on methylisocyanate and N,N'-dimethylcarbodiimide. Similarly, H-abstractions by OH show significant sensitivity coefficients. Although the developed model would benefit from more validations against experimental results, especially under combustion conditions, the current simulations reproduce the existing experimental data, giving good confidence in the proposed mechanism.

Supporting Information

Isodesmic reactions, detailed mechanism in Chemkin Pro format, NASA polynomials for all species.

Acknowledgments

This project has received funding from the region Grand-Est (project CATCH). High performance computing resources were provided by IDRIS under the allocation AD010812434R1 made by GENCI and also by the EXPLOR center hosted by the University of Lorraine.

References:

[1] P. Glarborg, J.A. Miller, B. Ruscic, S.J. Klippenstein, Modeling nitrogen chemistry in combustion, Progress in energy and combustion science 67 (2018) 31-68.

[2] L. Bengtström, M. Salden, A.A. Stec, The role of isocyanates in fire toxicity, Fire Science Reviews 5 (2016) 4.

[3] S. Sriramachari, The Bhopal gas tragedy: An environmental disaster, Curr. Sci. 86 (2004) 905-920.

[4] I. Eckerman, The Bhopal gas leak: Analyses of causes and consequences by three different models, Journal of Loss Prevention in the Process Industries 18 (2005) 213-217.

[5] D.K. Papanastasiou, F. Bernard, J.B. Burkholder, Atmospheric Fate of Methyl Isocyanate, CH3NCO: OH and Cl Reaction Kinetics and Identification of Formyl Isocyanate, HC(O)NCO, ACS Earth and Space Chemistry 4 (2020) 1626-1637.

[6] M.A. Garrido, A.C. Gerecke, N. Heeb, R. Font, J.A. Conesa, Isocyanate emissions from pyrolysis of mattresses containing polyurethane foam, Chemosphere 168 (2017) 667-675.

[7] P. Blomqvist, T. Hertzberg, M. Dalene, G. Skarping, Isocyanates, aminoisocyanates and amines from fires—a screening of common materials found in buildings, Fire Mater. 27 (2003) 275-294.

[8] J. Honorien, R. Fournet, P.-A. Glaude, B. Sirjean, Theoretical Study of the Thermal Decomposition of Urea Derivatives, J. Phys. Chem. A 126 (2022) 6264-6277.

[9] M. Risholm-Sundman, E. Vestin, Emissions during combustion of particleboard and glued veneer, European Journal of Wood and Wood Products 63 (2005) 179-185.

[10] M. Watanabe, C. Nakata, W. Wu, K. Kawamoto, Y. Noma, Characterization of semi-volatile organic compounds emitted during heating of nitrogen-containing plastics at low temperature, Chemosphere 68 (2007) 2063-2072.

[11] L. Jiang, D. Zhang, M. Li, J.-J. He, Z.-H. Gao, Y. Zhou, J.-H. Sun, Pyrolytic behavior of waste extruded polystyrene and rigid polyurethane by multi kinetics methods and Py-GC/MS, Fuel 222 (2018) 11-20.

[12] M.A. Garrido, R. Font, Pyrolysis and combustion study of flexible polyurethane foam, Journal of Analytical and Applied Pyrolysis 113 (2015) 202-215.
[13] M. Paabo, B.C. Levin, A review of the literature on the gaseous products and toxicity generated from the pyrolysis and combustion of rigid polyurethane foams, Fire and Materials 11 (1987) 1-29.
[14] S. Yurdakul, A. Atimtay, Investigation of emissions from thermal oxidation of waste wood samples using spectral methods, International Journal of Global Warming 7 (2015) 423-438.
[15] M.E. Bailey, V. Kirss, R.G. Spaunburgh, Reactivity of Organic Isocyanates, Industrial & Engineering Chemistry 48 (1956) 794-797.
[16] R.G. Arnold, J.A. Nelson, J.J. Verbanc, Recent Advances In Isocyanate Chemistry, Chemical Reviews 57 (1957) 47-76.
[17] P.G. Blake, S. Ijadi-Maghsoodi, Kinetics and mechanism of the thermal decomposition of methyl isocyanate, Int. J. Chem. Kinet. 14 (1982) 945-952.
[18] P.G. Blake, S. Ijadi-Maghsoodi, The kinetics and mechanism of thermal decomposition of alkyl isocyanates, Int. J. Chem. Kinet. 15 (1983) 609-618.
[19] S.T. Marks, E. Metcalfe, The pyrolysis of para-toluene isocyanate, Combust. Flame 107 (1996) 260-270.
[20] L. Goerigk, S. Grimme, Efficient and Accurate Double-Hybrid-Meta-GGA Density Functionals—Evaluation with the Extended GMTKN30 Database for General Main Group Thermochemistry, Kinetics, and Noncovalent Interactions, Journal of Chemical Theory and Computation 7 (2011) 291-309.
[21] S. Grimme, S. Ehrlich, L. Goerigk, Effect of the damping function in dispersion corrected density functional theory, J. Comput. Chem. 32 (2011) 1456-1465.
[22] M. Biczysko, P. Panek, G. Scalmani, J. Bloino, V. Barone, Harmonic and anharmonic vibrational frequency calculations with the double-hybrid B2PLYP method: analytic second derivatives and benchmark studies, Journal of Chemical Theory and Computation 6 (2010) 2115-2125.
[23] M.J. Frisch, G.W. Trucks, H.B. Schlegel, G.E. Scuseria, M.A. Robb, J.R. Cheeseman, G. Scalmani, V. Barone, G.A. Petersson, H. Nakatsuji, X. Li, M. Caricato, A.V. Marenich, J. Bloino, B.G. Janesko, R. Gomperts, B. Mennucci, H.P. Hratchian, J.V. Ortiz, A.F. Izmaylov, J.L. Sonnenberg, Williams, F. Ding, F. Lipparini, F. Egidi, J. Goings, B. Peng, A. Petrone, T. Henderson, D. Ranasinghe, V.G. Zakrzewski, J. Gao, N. Rega, G. Zheng, W. Liang, M. Hada, M. Ehara, K. Toyota, R. Fukuda, J. Hasegawa, M. Ishida, T. Nakajima, Y. Honda, O. Kitao, H. Nakai, T. Vreven, K. Throssell, J.A. Montgomery Jr., J.E. Peralta, F. Ogliaro, M.J. Bearpark, J.J. Heyd, E.N. Brothers, K.N. Kudin, V.N. Staroverov, T.A. Keith, R. Kobayashi, J. Normand, K. Raghavachari, A.P. Rendell, J.C. Burant, S.S. Iyengar, J. Tomasi, M. Cossi, J.M. Millam, M. Klene, C. Adamo, R. Cammi, J.W. Ochterski, R.L. Martin, K. Morokuma, O. Farkas, J.B. Foresman, D.J. Fox, Gaussian 16 Rev. B.01, Wallingford, CT, 2016.

[24] J. Pfaendtner, X. Yu, L. Broadbelt, The 1-D hindered rotor approximation, Theor Chem Account 118 (2007) 881-898.
[25] J. Lizardo-Huerta, B. Sirjean, R. Bounaceur, R. Fournet, Intramolecular effects on the kinetics of unimolecular reactions of β-HOROO˙ and HOQ˙ OOH radicals, PCCP 18 (2016) 12231-12251.
[26] F. Zhang, T.S. Dibble, Impact of tunneling on hydrogen-migration of the n-propylperoxy radical, PCCP 13 (2011) 17969-17977.
[27] B. Sirjean, E. Dames, H. Wang, W. Tsang, Tunneling in hydrogen-transfer isomerization of n-alkyl radicals, J. Phys. Chem. A 116 (2012) 319-332.
[28] NIST Computational Chemistry Comparison and Benchmark Database. http://cccbdb.nist.gov/.
[29] B. Ruscic, D.H. Bross, Active Thermochemical Tables (ATcT) values based on ver. 1.122p of the Thermochemical Network. https://atct.anl.gov/.
[30] Y. Georgievskii, J.A. Miller, M.P. Burke, S.J. Klippenstein, Reformulation and Solution of the Master Equation for Multiple-Well Chemical Reactions, J. Phys. Chem. A 117 (2013) 12146-12154.
[31] Reaction-Design, CHEMKIN 10112 (San Diego 2011).
[32] L.S. Tee, S. Gotoh, W.E. Stewart, Molecular Parameters for Normal Fluids. Lennard-Jones 12-6 Potential, Industrial & Engineering Chemistry Fundamentals 5 (1966) 356-363.
[33] J. Marrero, R. Gani, Group-contribution based estimation of pure component properties, Fluid Phase Equilib. 183 (2001) 183-208.
[34] C.J. Annesley, J.B. Randazzo, S.J. Klippenstein, L.B. Harding, A.W. Jasper, Y. Georgievskii, B. Ruscic, R.S. Tranter, Thermal Dissociation and Roaming Isomerization of Nitromethane: Experiment and Theory, J. Phys. Chem. A 119 (2015) 7872-7893.
[35] Y.R. Luo, Handbook of Bond Dissociation Energies in Organic Compounds, CRC press LLC2003.
[36] F. Buda, R. Bounaceur, V. Warth, P. Glaude, R. Fournet, F. Battin-Leclerc, Progress toward a unified detailed kinetic model for the autoignition of alkanes from C-4 to C-10 between 600 and 1200 K, Combust. Flame 142 (2005) 170-186.
[37] C.-W. Zhou, J.M. Simmie, K.P. Somers, C.F. Goldsmith, H.J. Curran, Chemical Kinetics of Hydrogen Atom Abstraction from Allylic Sites by 3O2; Implications for Combustion Modeling and Simulation, J. Phys. Chem. A 121 (2017) 1890-1899.
[38] T.D.J. D'Silva, A. Lopes, R.L. Jones, S. Singhawangcha, J.K. Chan, Studies of methyl isocyanate chemistry in the Bhopal incident, The Journal of Organic Chemistry 51 (1986) 3781-3788.
[39] A.J. Eskola, T.T. Pekkanen, S.P. Joshi, R.S. Timonen, S.J. Klippenstein, Kinetics of 1-butyl and 2-butyl radical reactions with molecular oxygen: Experiment and theory, Proc. Combust. Inst. 37 (2019) 291-298.
[40] T. Faravelli, A. Goldaniga, L. Zappella, E. Ranzi, P. Dagaut, M. Cathonnet, An experimental and kinetic modeling study of propyne and allene oxidation, Proc. Combust. Inst. 28 (2000) 2601-2608.

[41] S.G. Davis, C.K. Law, H. Wang, Propyne pyrolysis in a flow reactor: An experimental, RRKM, and detailed kinetic modeling study, J. Phys. Chem. A 103 (1999) 5889-5899.
[42] W. Tsang, Chemical kinetic data base for combustion chemistry part V. Propene, J. Phys. Chem. Ref. Data 20 (1991) 221-273.
[43] A.M. Dean, J.W. Bozzelli, Combustion chemistry of nitrogen, Gas-phase combustion chemistry, Springer2000, pp. 125-341.
[44] D. Baulch, C. Bowman, C.J. Cobos, R.A. Cox, T. Just, J. Kerr, M. Pilling, D. Stocker, J. Troe, W. Tsang, Evaluated kinetic data for combustion modeling: supplement II, J. Phys. Chem. Ref. Data 34 (2005) 757-1397.
[45] Fire Protection Guide to Hazardous Materials, National Fire Protection Association, Quincy, MA, 2002.
[46] Hazardous Substances Data Bank (HSDB). https://pubchem.ncbi.nlm.nih.gov/source/hsdb/1165.
[47] ASTM E 659–78, 1989, Standard test method for auto-ignition temperature of liquid chemicals, American Society for Testing and Materials, Philadelphia
[48] P.-A. Glaude, B. Sirjean, R. Fournet, R. Bounaceur, M. Vierling, P. Montagne, M. Molière, Combustion and oxidation kinetics of alternative gas turbines fuels, Turbo Expo: Power for Land, Sea, and Air 45653 (2014) V03AT03A001.
[49] A.A. Pekalski, E. Terli, J.F. Zevenbergen, S.M. Lemkowitz, H.J. Pasman, Influence of the ignition delay time on the explosion parameters of hydrocarbon–air–oxygen mixtures at elevated pressure and temperature, Proc. Combust. Inst. 30 (2005) 1933-1939.